

Polymer Fiber Probes Enable Optical Control of Spinal Cord and Muscle Function In Vivo

Chi Lu, Ulrich P. Froriep, Ryan A. Koppes, Andres Canales, Vittorio Caggiano, Jennifer Selvidge, Emilio Bizzi, and Polina Anikeeva*

Restoration of motor and sensory functions in paralyzed patients requires the development of tools for simultaneous recording and stimulation of neural activity in the spinal cord. In addition to its complex neurophysiology, the spinal cord presents technical challenges stemming from its flexible fibrous structure and repeated elastic deformation during normal motion. To address these engineering constraints, we developed highly flexible fiber probes, consisting entirely of polymers, for combined optical stimulation and recording of neural activity. The fabricated fiber probes exhibit low-loss light transmission even under repeated extreme bending deformations. Using our fiber probes, we demonstrate simultaneous recording and optogenetic stimulation of neural activity in the spinal cord of transgenic mice expressing the light sensitive protein channelrhodopsin 2 (ChR2). Furthermore, optical stimulation of the spinal cord with the polymer fiber probes induces on-demand limb movements that correlate with electromyographical (EMG) activity.

With the introduction of optogenetics,^[8,9] a method that permits on-demand excitation and inhibition of activity in optically-sensitized neurons with light pulses, integration of photonic modules into microelectronic neural recording probes yielded closed-loop sensor-actuator devices.^[10] These probes often combined optical fibers with established neural recording technologies such as silicon multielectrode arrays,^[11,12] multitrodes^[13,14] and tetrodes.^[15] Recently, microelectromechanical systems (MEMS) and contact printing fabrication methods allowed for innovative structures with multiple integrated modalities.^[16,17] These advances in optoelectronic neural probe technologies have helped further the understanding of brain circuits and contributed to the development of therapies

for neurological disorders.^[18–20] Fewer studies have explored application of optogenetics in the spinal cord.^[21–24] Specifically, despite pioneering in vitro efforts,^[21,22] direct control of limb movement via optical spinal cord stimulation in a live mammal has yet to be demonstrated.

The spinal cord is highly viscoelastic (elastic modulus of 0.5–1 MPa) and experiences up to ~10% of repeated strain during motion,^[25,26] presenting a challenge to combined intraspinal neural recording and optical stimulation, since the majority of neural probes and light-delivery devices are comprised of brittle materials^[27–29] that may cause damage to the neural tissue and fail under repeated deformation.^[30] To overcome these limitations, we engineered highly flexible biomimetic all-polymer fiber probes that combine an optical core for optogenetic stimulation and conductive electrodes for simultaneous neural recording.

1. Introduction

The mammalian spinal cord consists of a multitude of axonal fibers 1–20 μm in diameter that carry motor stimuli from the brain to the trunk and the limbs, and the sensory information from the limbs back to the central nervous system.^[1–3] Spinal cord injuries disrupt this information exchange leading to loss of voluntary movement.^[4] Consequently, there is a need for neuroprosthetic technologies that enable simultaneous input and output of neural signals to and from the spinal cord.^[5–7]

C. Lu, A. Canales, J. Selvidge, P. Anikeeva
Department of Materials Science and Engineering
Massachusetts Institute of Technology
Cambridge, MA 02139, USA
E-mail: anikeeva@mit.edu

C. Lu, U. P. Froriep, R. A. Koppes,
A. Canales, P. Anikeeva
Research Laboratory of Electronics
Massachusetts Institute of Technology
Cambridge, MA 02139, USA

U. P. Froriep
Simons Center for the Social Brain
Massachusetts Institute of Technology
Cambridge, MA 02139, USA

V. Caggiano, E. Bizzi
McGovern Institute for Brain Research
Massachusetts Institute of Technology
Cambridge, MA 02139, USA



2. Design and Fabrication

We employed thermal drawing to fabricate these bifunctional polymer fiber probes as it permits simultaneous processing of multiple materials.^[31–33] Control over the stress during the draw enables preservation of the cross-sectional geometry of the preform, a macroscopic template of the final device, while features are reduced by up to 200 times and the length is scaled accordingly, producing hundreds of meters of fiber.^[34]

DOI: 10.1002/adfm.201401266

To create flexible fiber probes for implantation into the spinal cord, we chose polycarbonate (PC, refractive index $n = 1.58$, glass transition temperature $T_g = 145$ °C, elastic modulus $E = 2.38$ GPa), and cyclic olefin copolymer (COC, $n = 1.52$, $T_g = 158$ °C, $E = 3.0$ GPa) for the optical core and cladding, respectively, due to the refractive index contrast and low absorption of both materials in the visible part of the spectrum.^[35–37] Carbon-black doped conductive polyethylene (CPE, $T_m = 120$ °C, resistivity $\rho = 3 \times 10^1$ Ω -cm) was used as a recording electrode material.

In addition to optical and electrical features, the preform was designed to incorporate a sacrificial PC cladding layer to establish stable drawing conditions, characteristic of thicker fibers (Figure 1a). We tuned the fiber diameter between 400–1100 μ m by adjusting the drawing speed (Figure 1b, Supplementary Figure S1). The resulting fiber features were reduced by 30–80 times from the preform dimensions (Figure 1c, d) and etching of the PC layer yielded a final fiber probe diameter in the range of 180–230 μ m. Using similar fabrication procedures we also produced pure PC and PC/COC fibers (140–400 μ m in diameter, Supplementary Figure S2).

3. Results and Discussion

Excitation of neurons expressing ChR2 (absorption peak at 473 nm) can be reliably achieved using blue light pulses at optical power densities of 1–50 mW/mm², frequencies ≤ 50 Hz, and pulse widths of 0.5–20 ms.^[8] We found that the transmission spectra of the PC/COC fibers in the visible range are relatively flat and match those of pure PC fibers with similar dimensions. Introduction of absorptive CPE electrodes lead to a transmission dip at 625–700 nm (Figure 2a).

Optical losses at $\lambda = 473$ nm were further quantified, by coupling laser light into PC/COC fibers of core diameters 65–120 μ m and length 0–13 cm (Figure 2b). We found that the loss coefficient increased from 1.07 ± 0.04 dB/cm in 120 μ m core fibers to 2.32 ± 0.12 dB/cm in 65 μ m core fibers. For a 90 μ m core PC/COC fiber, incorporation of CPE electrodes resulted in an increase of the loss coefficient from 1.48 ± 0.04 to 2.30 ± 0.02 dB/cm. The latter implies that the optical power densities needed for ChR2-facilitated neural excitation can be easily achieved with commonly available 50–100 mW laser diodes even at fiber probe lengths of >10 cm. The observed optical losses at 473 nm in our bifunctional PC/COC/CPE fiber probes are 3–6 times lower than those of commonly used photopatternable polymer waveguides, such as SU-8.^[16,38] Furthermore, PC/COC/CPE fiber probes are not limited to flat substrate geometry and can be made arbitrarily long, enabling them to not only conform to the anatomical features of the spinal cord, but also translate with features under normal motion.

The bending stiffness of these polymer fiber probes (diameter 220 μ m, length 12.5 mm), measured in a single cantilever setup with 50 μ m bending deformation, is an order of magnitude lower than that of a conventional silica fiber with similar diameter and length (240 μ m silica fiber with polymer cladding) in a single cantilever mode in a frequency range of 0.01–10 Hz, characteristic of mammalian locomotion, respiration, and heartbeat (Figure 3a). Silica fibers without polymer

cladding rapidly fractured before completing the measurement (results not shown).

We have evaluated the performance of fiber probes under mechanical deformation, which commonly occurs in the spinal cord during motion. Optical losses at $\lambda = 473$ nm were measured at deformation angles of 90°, 180°, and 270° with radii of curvature 0.5–15 mm (Figure 3b). Approximately 25% transmission was observed at 270° with 0.5 mm radius of curvature, which is impossible with glass fibers. To ensure no degradation of optical performance occurs under repeated strain during locomotion, we performed a 15-cycle experiment with 180° deformation at 2.5 mm radius of curvature and did not observe an appreciable decline in performance (Figure 3c). Consequently, the observed increase in loss during bending deformation (Figure 3b) can be solely attributed to an increased scattering and coupling into the cladding rather than to permanent damage to the structure.

In addition to light guidance, fiber probes are designed to perform simultaneous electrical recording of neural activity. Impedance spectroscopy in a frequency range of 10 Hz–10 kHz (Figure 4, and Supplementary Figure S3) showed that PC/COC/CPE fiber probes exhibit slightly decreasing impedance values of 1.3 – 2.8 ± 0.4 M Ω (for 10 mm) and 2 – 6 ± 2 M Ω (for 50 mm) at 10–1000 Hz (the frequency range most useful for recording of neuronal activity), which lies within the range commonly cited for neural probes.^[29,39,40]

We evaluated the fiber probes shown in Figure 1c in the lumbar spinal cord (300 μ m deep) of transgenic Thy1-ChR2-YFP mice expressing ChR2 fused to the yellow fluorescent protein (YFP) across the excitatory nervous system,^[41] which includes the spinal cord (Supplementary Figure S4). Laser pulses (473 nm, 32 mW/mm², 5 ms pulse width, 10 Hz, 1 s epochs, 5 s interval) delivered through the PC core of the fiber probe robustly evoked neural activity in the spinal cord, as recorded with the CPE electrodes integrated within the same device (Figures 5a, b and Supplementary Figures S5&6). To confirm the physiological nature of the optically evoked activity we performed stimulation at 100 Hz (Supplementary Figure S7&8), producing initial increase in neural activity, followed by decreased activity without temporal correlation to the laser pulses, consistent with previous reports.^[15,42] Furthermore, to control for optoelectronic artifacts that sometimes occur in optogenetic experiments,^[43] we have tested our devices in wild type mice that do not express ChR2, where they showed an ability to record neural activity corresponding to sensory stimulation (toe pinch), but did not optically evoke activity (Supplementary Figure S9).

Optical activation of the lumbar spinal cord circuitry corresponded to lower limb muscle activation indicated by twitches that closely correlated to the laser pulses (Figure 5c–e and Supplementary online video). Based on previous reports, we hypothesize, that optical stimulation of the spinal cord leads to the activation of motoneuron fibers through the sciatic nerve leading to the recruitment of motor units within the gastrocnemius muscle.^[44] To quantify the optically evoked muscle activity we performed EMG recordings during 120 s of 1 Hz optical stimulation with 5 ms pulse width (Figure 5c, d). The envelopes of the EMG waveforms were temporally correlated to laser pulses with a time delay of 10.6 ± 2.3 ms (mean \pm s.d.) (Figure 5e).

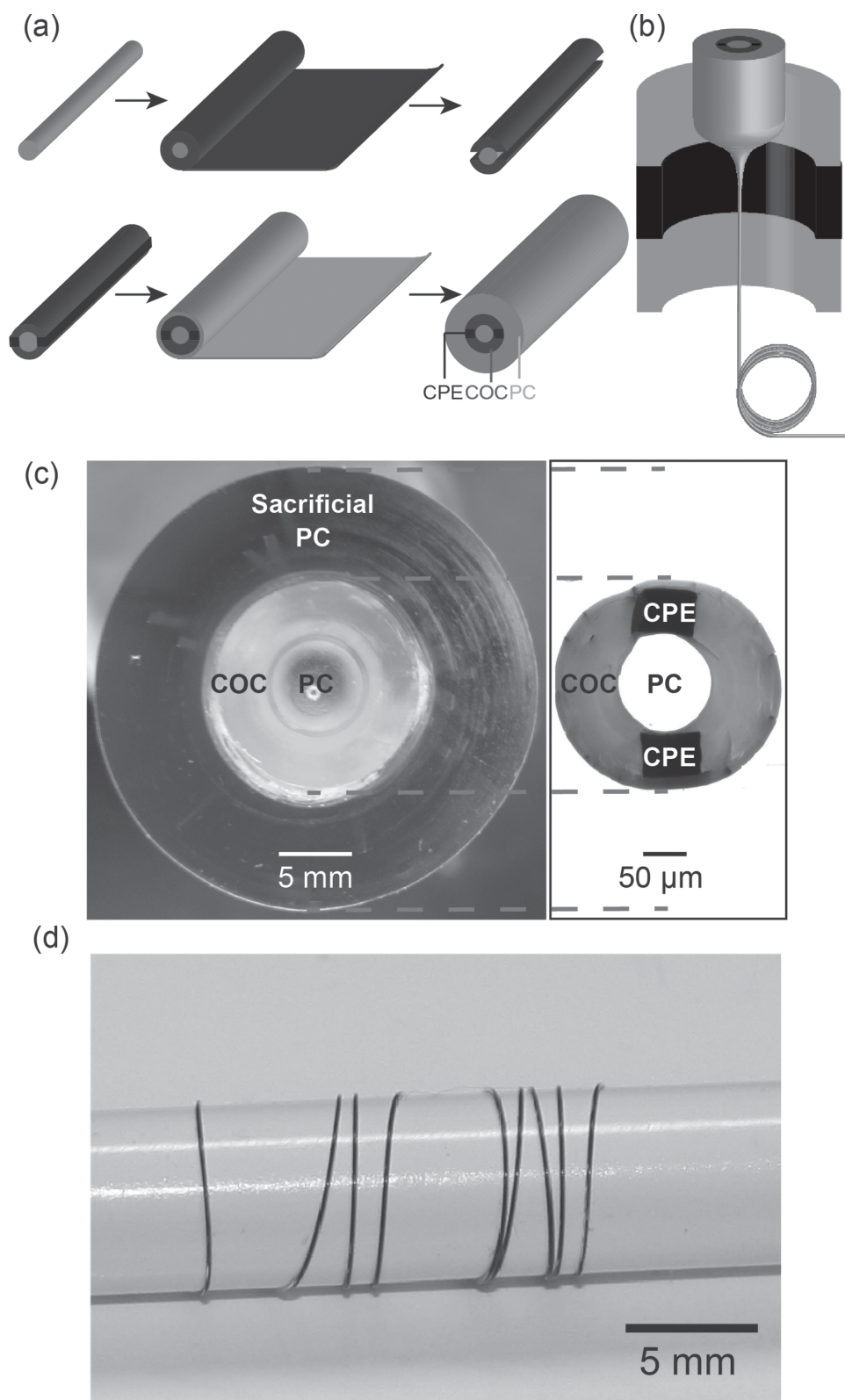


Figure 1. Fabrication process of all-polymer neural fiber probes. a) An illustration of the preform fabrication steps. b) A schematic showing the drawing of the preform into a fiber by applied heat. c) Left: A photograph of the cross section of the preform comprising the PC core, COC cladding, CPE electrodes and a sacrificial PC layer surrounding the entire structure. Right: A microscope image of the cross-section of the polymer neural probe produced from the preform following the etching of the PC sacrificial layer. The diameter reduction after drawing was 80 times, resulting in 850 m of fiber with a conserved cross section. d) A photograph of the etched PC/COC/CPE fiber wrapped around a pencil.

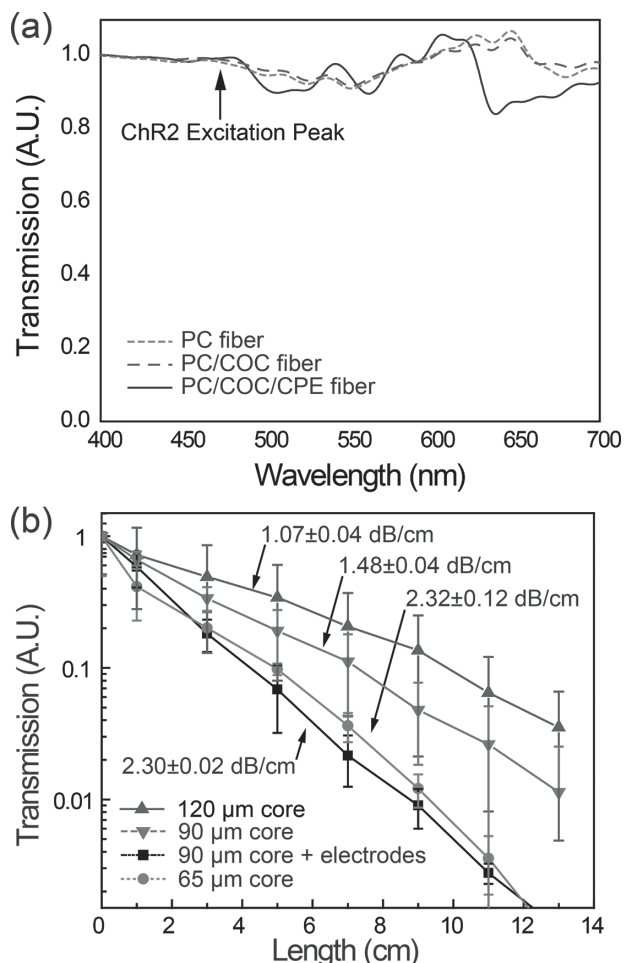


Figure 2. Optical characteristics of the fiber probe. a) Normalized transmission spectra measured in the visible range (400–700 nm) for PC and PC/COC fibers. b) Normalized transmission of PC/COC (core diameters 65 μm , 90 μm and 120 μm) and PC/COC/CPE (core diameter 90 μm) fibers shown for fiber lengths of 0–13 cm. Optical loss coefficients (dB/cm) increase with decreasing core diameter as well as with the incorporation of absorptive CPE electrodes next to the PC core.

4. Conclusion

Applying a fiber drawing process to a materials set consisting exclusively of polymers, we produced highly flexible miniature bifunctional neural probes for simultaneous optical stimulation and electrical neural recording in the spinal cord in vivo. Our fiber probes exhibit low optical losses and maintain their functionality at deformation angles up to 270°, radii of curvature as small as 500 μm , and following repeated loading. These devices have relatively flat transmission spectra across the visible spectrum, and thus can also be used for optical neural interrogation involving light-sensitive proteins (opsins) with activation spectra in the yellow or green parts of the visible spectrum. Our experiments in live mice illustrate the utility of the fiber probes for optical control of motor functions via optogenetic stimulation of the spinal cord, allowing the correlation of evoked neural activity to a behavioral response. Consequently, our all-polymer fiber probes provide a step towards the development of flexible biomimetic optoelectronic neuroprosthetics.

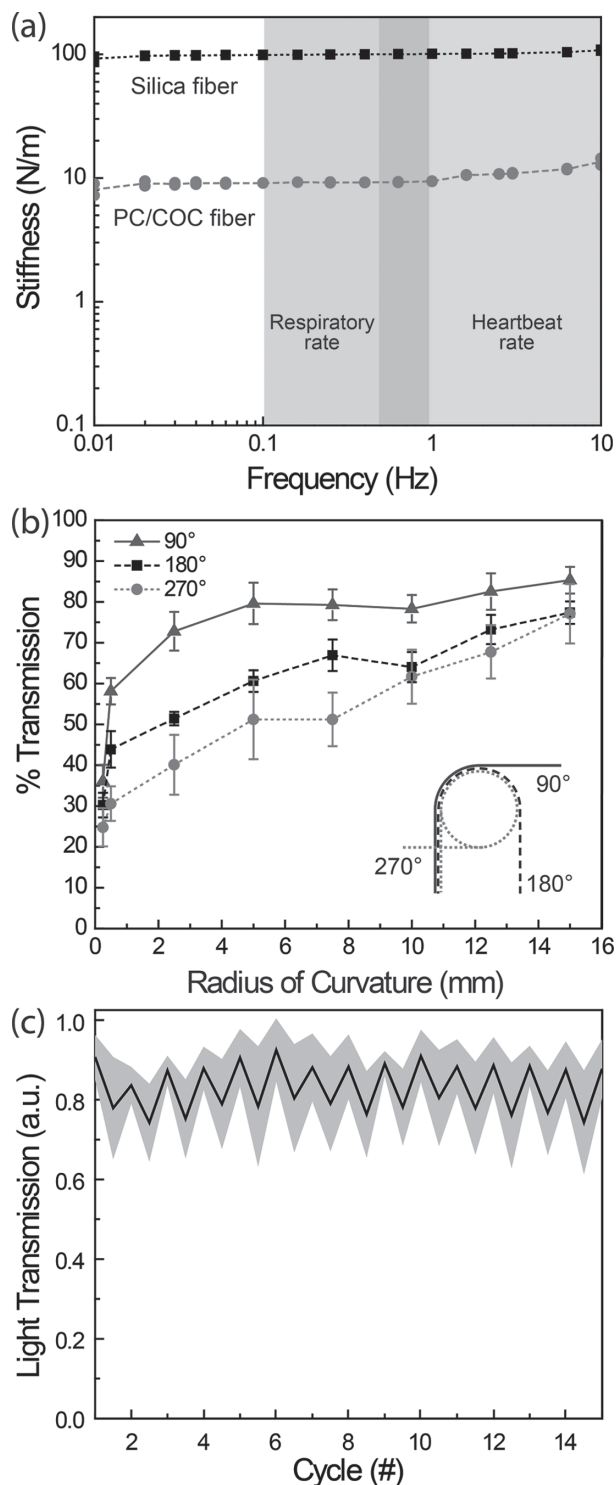


Figure 3. Mechanical characteristics of the fiber probe. a) Bending stiffness of PC/COC and commercially available silica fiber (diameters = 220 and 240 μm , respectively). b) Relative optical transmission through the PC-COC-CPE fibers at 90°, 180°, 270° deformation with radii of curvature of 0.5–14 mm. Transmission shown as a percentage of optical power transmitted through a deformed device as compared to a straight device. c) Retained transmission for cycling tests done at 180° angle and radius of curvature = 2.5 mm shows that the optical transmission properties are not affected by repeated stress loading.

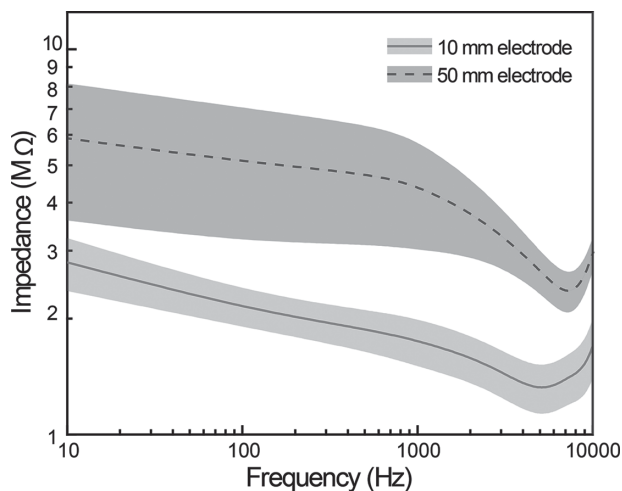


Figure 4. Embedded CPE electrode impedance. Impedance spectroscopy for PC/COC/CPE fiber probes of lengths 10 mm and 50 mm (10 Hz–10 kHz) shown as a mean (line) and standard deviation (shaded area).

5. Experimental Section

Fiber Probe Fabrication: To fabricate a preform, a polycarbonate (PC) cylinder (diameter = 0.25", McMaster Carr) was wrapped in cyclic olefin copolymer (COC) sheets (thickness = 0.002", TOPAS Advanced Polymers, 6014S) until the total diameter of the preform reached 14.8 mm. The entirety was then consolidated at 190 °C for 12 minutes in vacuum. After consolidation, two pockets ($L \times W \times H = 10 \text{ mm} \times 3.53 \text{ mm} \times 4 \text{ mm}$) at symmetrical positions on the surface of the preform were machined and filled with conductive polyethylene slabs (Hillas Packaging, CPE). The entire preform was then tightly wrapped in additional COC and PC sheets until the final outer diameter reached 32.1 mm to ensure that the preform was thick enough for stable drawing. The final preform was consolidated as described above. The fiber was drawn at 240 °C and the size of the preform was reduced by 40–80 times. Sacrificial PC cladding was etched away with dichloromethane (Sigma Aldrich) to further reduce the final size of the fiber probes.

Fiber Connections: The etched fibers were connected to zirconia ferrules (Thorlabs, CF270) using optical epoxy (Thorlabs, F112). The ferrule ends of the fibers were then polished with silicon-carbide sandpaper. The CPE electrodes were exposed by carefully removing the COC cladding, and connected to copper wire using conductive silver paint (SPI Supplies, 04998AB), and then sealed with epoxy (Devcon, 5 Minute® Epoxy). The copper electrode leads were then connected to a 16-channel ZIF connector (Tucker Davis Technologies (TDT)) for electrophysiological data acquisition. Prior to implantation, the fiber probes were cleaned and the connecting points between the ferrule and the probe, and the copper wire and the probe were encapsulated in epoxy (Supplementary Figure S10).

Optical Characterization: The optical transmission spectra were measured using a broadband spectrometer (Ocean Optics Inc., HR2000CG-UV-NIR) connected to a computer and calibrated with a white light source (Anritsu, MG922A). We assessed optical loss coefficients (in dB/cm) by coupling the fibers to a 473 nm blue laser (Laserglow Technologies) via ferrule-to-ferrule connection with zirconia sleeves (Thorlabs, ADAF1) and measuring the output power with a calibrated silicon photodiode (Thorlabs, S121C and PM100D).

Tests for light transmission at various bending angles and radii of curvature were performed using a custom machined mold designed to fit fiber probes of diameters of up to 300 μm . Cycling tests were performed by fixing one end of the fiber on a custom built stage and varying the radii of curvature with a translation stage (Thorlabs, PT3).

Mechanical Characterization: Mechanical tests were performed using a dynamic mechanical analyzer (TA Instruments, DMA Q800) in

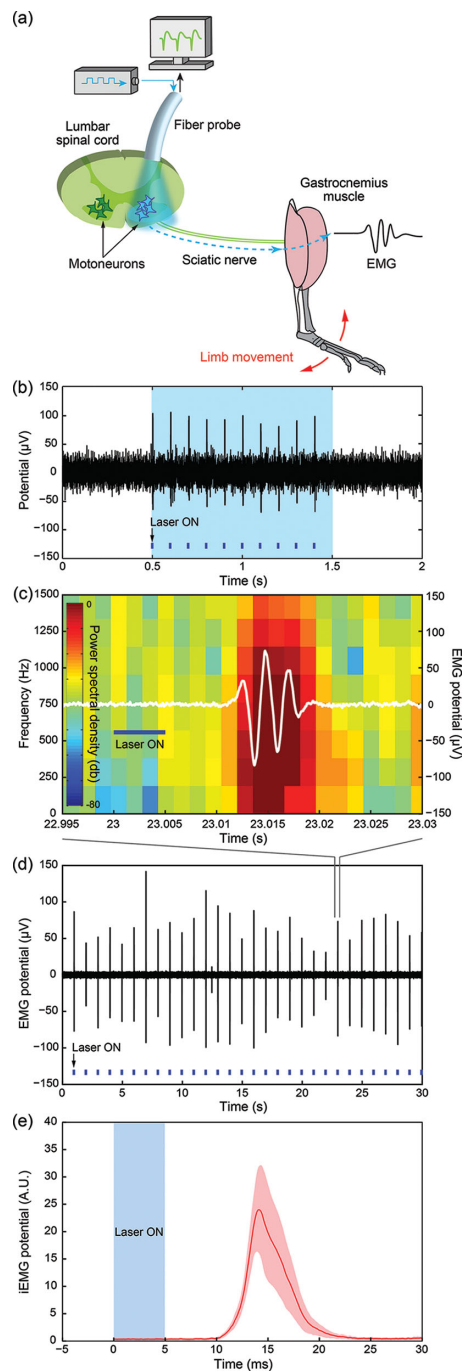


Figure 5. Control over spinal cord neural activity and limb movement. a) Schematic of the experimental setup. Optical stimulation of motoneurons likely activates the gastrocnemius muscle via the sciatic nerve. To quantify the onset of muscle activity, we performed EMG recordings. b) Neural activity in the spinal cord evoked by 10 Hz optical stimulation (wavelength $\lambda = 473 \text{ nm}$, 5 ms pulse width). c) Example EMG trace (white, right y-axis) closely following the optical stimulus (blue), superimposed on the EMG spectrogram (left y-axis). The signal exhibits a high power up to 1500 Hz. d) Continuous stimulation at 1 Hz reliably activated the muscle. e) Integrated EMG (iEMG, $n = 120$ trials, mean (line) \pm SD (shaded area)) after filtering (3–3000 Hz) and rectification confirmed the reliability of the muscle activation and accuracy of the EMG recordings.

a sinusoidal single cantilever setup with a sample length of 12.7 mm, deflection amplitude of 50 μm , and frequency range of 0.01–10 Hz.

Electrode Characterization: Tip impedance values of CPE electrodes were measured with a custom built voltage divider circuit attached to a RZ5D recording system (TDT), which was programmed to provide a sinusoidal signal (± 8 V, 1 kHz). Impedance was then calculated from the measured voltage drop across the electrodes for a frequency range of 0.01–10 kHz.

Recording and Optical Stimulation of Spinal Cord Neurons: All procedures involving animals were approved by the MIT Committee on Animal Care. The fiber probes were tested in male Thy1-ChR2-YFP mice generously provided by Guoping Feng, MIT, and housed at the MIT central animal facility (12h light/dark cycle, 22 °C, food and water ad libitum).

Mice were deeply anesthetized (in mg/kg bodyweight: ketamine: 100, xylazine: 10, in 0.9% sterile saline) and placed in a stereotactic frame (David Kopf Instruments) during surgeries. Connection to the RZ5D recording system was established via a PZ2-32 headstage with a ZIF-clip attached to a Headstage-To-Acute-Probe Adapter (TDT). The T12 vertebrae, which is rostral to the lumbar section of the mouse spinal cord, was used as an anatomical reference. Fiber probes were inserted 300 μm deep into the left proximal lumbar section of the cord. The depth was measured relative to the cord surface by the stereotactic micropositioners.

Optogenetic stimulation: Using a custom-built optical setup, we coupled a 473 nm laser (Laserglow Technologies) into a 2 m-long multimode silica fiber (50 μm diameter, Thorlabs, FG050UGA) “extension cord” and then coupled it to the fiber probe via a ferrule-to-ferrule connection with a zirconia sleeve. Fiber probes were then placed in a device holder for the stereotactic frame. Stimulation frequencies were controlled using the RZ5D system (10, 100 Hz; 5 ms pulse duration, 1 s trial duration, 5 s inter-trial interval, 20 trials, stimulation power 32 mW/mm²).

Neural recording: Electrophysiological data from the spinal cord was collected via the implanted fiber probe. A stainless steel wire (Goodfellow, FE245840) was used as ground wire and positioned under the skin around the neck while a channel without apparent electrophysiological signals was used as a secondary reference. The signal was filtered (0.3 – 10 kHz) and digitized (~ 50 kHz sampling frequency). Data analysis was performed in Matlab using built-in and custom written functions. To quantify reliable neural stimulation in the spinal cord, we applied a threshold on the recorded signal and calculated peri-stimulus time histograms (PSTH) across 20 trials (Supplementary Figure S6).

Electromyographical (EMG) recording: EMG data was acquired via two stainless steel electrodes (A-M Systems, 0.002"/0.0045" Bare/Coated) inserted into the belly of the gastrocnemius muscle (Figure 5a) and near the muscle-tendon junction of the Achilles tendon. EMG leads were connected to the PZ2-32 headstage (1 Hz–10 kHz filter settings, ~ 50 kHz sampling frequency). Spectrograms were calculated in Matlab using data sections of 100 data points with an overlap of 25% (Figure 5c). Since spectrograms revealed high power up to 1.5 kHz, we filtered the signal (3 Hz–3 kHz, symmetrical 2nd order Butterworth filter) and calculated integrated EMGs (iEMG) by isolating EMG trials, subtracting the mean from each trial, and subjecting the result to a Hilbert transformation to calculate the analytical signal. The real and the imaginary part of the analytical signal were squared, the results summed, and the square root of the sum resulted in the envelope constituting the iEMG (Figure 5e and Supplementary Figure S11). We assessed the time delay between the laser pulse and the EMG onset by applying a threshold to the data, and considering the first crossing of that threshold as onset of muscle activity, followed by calculation of mean and SD in Matlab. The threshold was defined as the mean of ‘noise’ activity (200 ms after one laser pulse to 200 ms before the next pulse) for all trials and adding the corresponding four standard deviations to that value.

Supporting Information

Supporting Information is available from the Wiley Online Library or from the author.

Acknowledgements

This work was supported by the National Science Foundation (NSF) under EEC-1028725, CAREER Award to PA and DMR-0819762, a McGovern Institute for Brain Research Neurotechnology grant, and by a grant from the Simons Foundation to the Simons Center for the Social Brain at MIT. We thank Prof. Yoel Fink for kindly providing access to the fiber-drawing tower. The authors also thank Prof. Guoping Feng for generously providing Thy1-ChR2-YFP mice.

Received: April 19, 2014

Revised: June 10, 2014

Published online:

- [1] E. Pierrot-Deseilligny, D. Burke, *The circuitry of the human spinal cord: its role in motor control and movement disorders*, Cambridge University Press, **2005**.
- [2] D. Debanne, E. Campanac, A. Bialowas, E. Carlier, G. Alcaraz, *Physiol. Rev.* **2011**, *91*, 555.
- [3] S. Grillner, T. M. Jessell, *Curr. Opin. Neurobiol.* **2009**, *19*, 572.
- [4] S. Thuret, L. D. Moon, F. H. Gage, *Nat. Rev. Neurosci.* **2006**, *7*, 628.
- [5] J. Schouenborg, M. Garwicz, N. Danielsen, *Brain Machine Interfaces: Implications for Science, Clinical Practice and Society* **2011**, *194*, 47.
- [6] V. R. Edgerton, S. Harkema, *Expert Rev. Neurother.* **2011**, *11*, 1351.
- [7] S. E. Mondello, M. R. Kasten, P. J. Horner, C. T. Moritz, *Front. Neurosci.* **2014**, *8*, 21.
- [8] O. Yizhar, L. E. Fenno, T. J. Davidson, M. Mogri, K. Deisseroth, *Neuron* **2011**, *71*, 9.
- [9] F. Zhang, A. M. Aravanis, A. Adamantidis, L. de Lecea, K. Deisseroth, *Nat. Rev. Neurosci.* **2007**, *8*, 577.
- [10] R. Pashaie, P. Anikeeva, J. Lee, R. Prakash, O. Yizhar, *IEEE Rev. Biomed. Eng.* **2014**, *7*, 3.
- [11] J. Zhang, F. Laiwalla, J. A. Kim, H. Urabe, R. Van Wagenen, Y. K. Song, B. W. Connors, F. Zhang, K. Deisseroth, A. V. Nurmikko, *J. Neural Eng.* **2009**, *6*, 055007.
- [12] J. Wang, F. Wagner, D. A. Borton, J. Zhang, I. Ozden, R. D. Burwell, A. V. Nurmikko, R. van Wagenen, I. Diester, K. Deisseroth, *J. Neural Eng.* **2012**, *9*, 016001.
- [13] M. Im, I.-J. Cho, F. Wu, K. D. Wise, E. Yoon, 2011 IEEE 24th Int. Conf. Micro Electro Mech. Syst. (MEMS), **2011**, 1051.
- [14] S. Royer, B. V. Zemelman, M. Barbic, A. Losonczy, G. Buzsaki, J. C. Magee, *Eur. J. Neurosci.* **2010**, *31*, 2279.
- [15] P. Anikeeva, A. S. Andalman, I. Witten, M. Warden, I. Goshen, L. Grosenick, L. A. Gunaydin, L. M. Frank, K. Deisseroth, *Nat. Neurosci.* **2012**, *15*, 163.
- [16] B. Rubehn, S. B. Wolff, P. Tovote, A. Luthi, T. Stieglitz, *Lab Chip* **2013**, *13*, 579.
- [17] T. I. Kim, J. G. McCall, Y. H. Jung, X. Huang, E. R. Siuda, Y. Li, J. Song, Y. M. Song, H. A. Pao, R. H. Kim, C. Lu, S. D. Lee, I. S. Song, G. Shin, R. Al-Hasani, S. Kim, M. P. Tan, Y. Huang, F. G. Omenetto, J. A. Rogers, M. R. Bruchas, *Science* **2013**, *340*, 211.
- [18] M. R. Warden, A. Selimbeyoglu, J. J. Mirzabekov, M. Lo, K. R. Thompson, S. Y. Kim, A. Adhikari, K. M. Tye, L. M. Frank, K. Deisseroth, *Nature* **2012**, *492*, 428.
- [19] A. V. Kravitz, B. S. Freeze, P. R. Parker, K. Kay, M. T. Thwin, K. Deisseroth, A. C. Kreitzer, *Nature* **2010**, *466*, 622.
- [20] J. J. Letzkus, S. B. Wolff, E. M. Meyer, P. Tovote, J. Courtin, C. Herry, A. Lüthi, *Nature* **2011**, *480*, 331.

- [21] M. Hagglund, L. Borgius, K. J. Dougherty, O. Kiehn, *Nat. Neurosci.* **2010**, *13*, 246.
- [22] M. Hagglund, K. J. Dougherty, L. Borgius, S. Itohara, T. Iwasato, O. Kiehn, *Proc. Natl. Acad. Sci. U.S.A.* **2013**, *110*, 11589.
- [23] C. Wyart, F. Del Bene, E. Warp, E. K. Scott, D. Trauner, H. Baier, E. Y. Isacoff, *Nature* **2009**, *461*, 407.
- [24] W. J. Alilain, X. Li, K. P. Horn, R. Dhingra, T. E. Dick, S. Herlitze, J. Silver, *J. Neurosci.* **2008**, *28*, 11862.
- [25] R. J. Fford, L. E. Bilston, *J. Biomech.* **2005**, *38*, 1509.
- [26] S. Cheng, E. C. Clarke, L. E. Bilston, *Med. Eng. Phys.* **2008**, *30*, 1318.
- [27] H. Wark, R. Sharma, K. Mathews, E. Fernandez, J. Yoo, B. Christensen, P. Tresco, L. Rieth, F. Solzbacher, R. Normann, *J. Neural Eng.* **2013**, *10*, 045003.
- [28] D. R. Sparta, A. M. Stamatakis, J. L. Phillips, N. Hovelso, R. van Zessen, G. D. Stuber, *Nat. Protoc.* **2012**, *7*, 12.
- [29] N. G. Hatsopoulos, J. P. Donoghue, *Annu. Rev. Neurosci.* **2009**, *32*, 249.
- [30] A. Prasad, J. C. Sanchez, *J. Neural Eng.* **2012**, *9*, 026028.
- [31] A. F. Abouraddy, M. Bayindir, G. Benoit, S. D. Hart, K. Kuriki, N. Orf, O. Shapira, F. Sorin, B. Temelkuran, Y. Fink, *Nat. Mater.* **2007**, *6*, 336.
- [32] S. Danto, Z. Ruff, Z. Wang, J. D. Joannopoulos, Y. Fink, *Adv. Funct. Mater.* **2011**, *21*, 1095.
- [33] A. Yildirim, M. Yunusa, F. E. Ozturk, M. Kanik, M. Bayindir, *Adv. Funct. Mater.* **2014**.
- [34] T. Izawa, S. Sudo, T. Izawa, **1987**.
- [35] M. Aden, A. Roesner, A. Olowinsky, *J. Polym. Sci., Part B: Polym. Phys.* **2010**, *48*, 451.
- [36] P. M. van Midwoud, A. Janse, M. T. Merema, G. M. Groothuis, E. Verpoorte, *Anal. Chem.* **2012**, *84*, 3938.
- [37] G. Khanarian, *Opt. Eng.* **2001**, *40*, 1024.
- [38] B. Bilenberg, T. Nielsen, B. Clausen, A. Kristensen, *J. Micromech. Microeng.* **2004**, *14*, 814.
- [39] K. Watanabe, T. Watanabe, H. Watanabe, H. Ando, T. Ishikawa, K. Kobayashi, *IEEE Trans. Biomed. Eng.* **2005**, *52*, 2100.
- [40] J. C. Williams, J. A. Hippensteel, J. Dilgen, W. Shain, D. R. Kipke, *J. Neural Eng.* **2007**, *4*, 410.
- [41] B. R. Arenkiel, J. Peca, I. G. Davison, C. Feliciano, K. Deisseroth, G. J., Augustine, M. D. Ehlers, G. Feng, *Neuron* **2007**, *54*, 205.
- [42] H. Liske, X. Qian, P. Anikeeva, K. Deisseroth, S. Delp, *Sci. Rep.* **2013**, *3*.
- [43] J. A. Cardin, M. Carlen, K. Meletis, U. Knoblich, F. Zhang, K. Deisseroth, L. H. Tsai, C. I. Moore, *Nat. Protoc.* **2010**, *5*, 247.
- [44] M. E. Llewellyn, K. R. Thompson, K. Deisseroth, S. L. Delp, *Nat. Med.* **2010**, *16*, 1161.